Clim Dyn
DOI 10.1007/s00382-007-0353-7

The relative importance of tropical variability forced from the North Pacific through ocean pathways

Amy Solomon · Sang-Ik Shin · Michael A. Alexander · Julian P. McCreary

Received: 11 June 2007 / Accepted: 4 December 2007

Abstract To what extent is tropical variability forced from the North Pacific through ocean pathways relative to locally generated variability and variability forced through the atmosphere? To address this question, in this study we use an anomaly-coupled model, consisting of a global, atmospheric general circulation model and a 4½-layer, reduced-gravity, Pacific-Ocean model. Three solutions are obtained; with coupling over the entire basin (CNT), with coupling confined to the tropics and wind stress and heat fluxes in the North and South Pacific specified by climatology (TP), and with coupling confined to the Tropics and wind stress and heat fluxes in the North Pacific specified by output from CNT (NPF). It is found that there are two distinct signals forced in the North Pacific that can impact the tropics through ocean pathways. These two signals are forced by wind stress and surface heat flux anomalies in the subtropical North Pacific. The first signal is relatively fast, impacts tropical variability less than a year after forcing, is triggered from November to March, and propagates as a first-mode baroclinic Rossby wave. The second signal is only triggered during springtime when buoyancy forcing can effectively generate higher-order baroclinic modes through subduction anomalies into the permanent thermocline, and it reaches the equator 4–5 years after forcing. The slow signal is found to initiate tropical variability more efficiently than the fast signal with one standard deviation in subtropical zonal wind stress forcing tropical SST anomalies centered on the equator at 135°W of approximately 0.5°C. Allowing extratropically forced tropical variability is found to shift primarily 2-year ENSO variability in a tropics-alone simulation to a more realistic range of 2–6 years.

A. Solomon (✉) · S.-I. Shin · M. A. Alexander
Physical Sciences Division,
NOAA/Earth System Research Laboratory,
R/PSD1, 325 Broadway, Boulder,
CO 80305-3328, USA
e-mail: Amy.Solomon@noaa.gov

A. Solomon · S.-I. Shin
CIRES Climate Diagnostics Center, Boulder, CO, USA

J. P. McCreary
International Pacific Research Center,
University of Hawaii, Honolulu, HI, USA

1 Introduction

A major challenge in climate science is to predict variations in tropical Pacific sea surface temperatures (SSTs) on interannual-to-decadal timescales. These SSTs impact climate globally by changing large-scale atmospheric circulation patterns. The motivation of this study is to improve our understanding of how tropical Pacific SSTs are affected by extratropical atmospheric variability through ocean pathways, commonly referred to as "the ocean bridge".

Several observational studies have suggested that there is a link between extratropical Pacific decadal variability and tropical Pacific interannual-to-decadal variability (Trenberth 1990; Latif et al. 1997; Zhang et al. 1998; Kleeman and Power 1999). For example, the results of Wang (1995) suggest that concurrent with the observed 1970s ''climate shift'' in the North Pacific (Nitta and Yamada 1989; Trenberth 1990; Deser et al. 2004) there

was an interdecadal change in the background state of the tropical Pacific that changed the onset of ENSO events, limiting predictability in coupled models (Ji et al. 1996).[1]

To date, several mechanisms have been proposed for the generation of tropical interannual-to-decadal variability forced from the extratropics, such as, oceanic teleconnections from the extratropics to the tropics, and, atmospheric teleconnections from the extratropics to the Tropics (e.g., Barnett et al. 1999). Atmospheric teleconnections from the extratropics are essentially changes in large-scale atmospheric circulation patterns over the Pacific Basin that project onto the equatorial region either directly or through coupled air–sea feedbacks in the subtropics, a process referred to as "seasonal footprinting" (Vimont et al. 2001). The atmospheric variability in seasonal footprinting is primarily forced by midlatitude internal atmospheric variability of stochastic origin.

Oceanic teleconnections from the extratropics are thought to follow subtropical cell pathways (STCs). STCs are shallow wind driven meridional cells that provide a pathway by which extratropical atmospheric variability can force tropical variability through the ocean. These cells are observed to exist in both the Pacific (e.g., Johnson and McPhaden 1999) and Atlantic (e.g., Zhang et al. 2003). Water in the STCs travels downward along isopycnal surfaces in the subtropics, flows equatorward within the thermocline, upwells in the eastern equatorial ocean, and flows out of the Tropics within a surface layer (Fig. 2 of Bryan 1991; McCreary and Lu 1994; Liu et al. 1994, 1998; Rothstein et al. 1998).

STC transport is determined largely by Ekman transport across the edge of the tropical warm pool (18–25°N) (McCreary and Lu 1994). Transport variability at the downward flowing, poleward edge of the STC is driven by a change in the mass flux from the mixed layer into the permanent thermocline. It is primarily driven by subduction in the region where isopycnals that intersect the equatorial undercurrent outcrop in the subtropics (e.g., Liu 1999). This diabatic pumping generates higher-order baroclinic oceanic Rossby waves that propagate equatorward along advective pathways (e.g., Thompson and Ladd 2004).

STC variability can force tropical decadal variability by temperature anomalies that subduct in the extratropics and upwell at the equator (Gu and Philander 1997) and/or by transport anomalies, due to subtropical wind stress anomalies, that change the amount of water that upwells at the equator (Kleeman et al. 1999). In this paper, STC variability refers to any change in more than one branch of the STCs even if the forcing is too weak or too fast to completely spin-up the cell.

Gu and Philander (1997) hypothesized that North Pacific SST anomalies are subducted into the thermocline and subsequently advected to the equatorial Pacific with a time lag of the order of a decade. This idea received observational support from Deser et al. (1996), who were able to follow the equatorward movement of a subsurface anomaly for some distance. However, the significance of this mechanism in generating tropical decadal variability is still uncertain since some OGCM solutions show that subtropical buoyancy forcing can significantly impact the equatorial thermocline through baroclinic Rossby wave propagation (Lysne et al. 1997; Shin and Liu 2000), while others show the signal attenuates by an order of magnitude by the time it reaches the equator (Schneider et al. 1999; Nonaka and Xie 2003) or recirculates within the subtropical gyre (e.g., Nonaka et al. 2006).

Kleeman et al. (1999) hypothesized that ENSO was modulated on decadal timescales by northern STC transport variability. These ideas are supported by the modeling study of Nonaka et al. (2002) and the observational study of McPhaden and Zhang (2002), which found a correspondence between a decrease in transport in the lower branch of the Pacific STCs and an increase in tropical Pacific SSTs since the 1970s, suggesting that transport variations in the Pacific STCs are driving tropical decadal variability.

In addition, Kleeman et al. (1999) hypothesized that STC transport variability is independent of tropical variability. In a related study, Solomon et al. (2003) found an alternative mechanism for maintaining STC transport variability composed of both atmospheric and oceanic bridges. Specifically, atmospheric teleconnections from the tropics to the extratropics forced by tropical decadal SST variability maintained the subtropical wind stress variability at the poleward edge of the STC while oceanic teleconnections from the extratropics to the Tropics maintained the tropical decadal variability.

There are also questions concerning the impact of STC variability on ENSO. Does STC variability cause a modulation of ENSO on decadal timescales without changing its frequency as was found by Kleeman et al. (1999)? Does STC variability cause decadal variations in the zonal mean equatorial thermocline depth and therefore a change in the frequency of ENSO as suggested by Federov and Philander (2001)? Or does STC variability change the spatial structure of ENSO (and a resultant change in ENSO frequency) as suggested by the eastward shift of the equatorial zonal wind stress anomalies with respect to the SST anomalies after the 1970's climate shift (An and Wang 2000)?

[1] Here we define tropical decadal variability as the variations in the tropical climate with timescales between 7 and 20 years. ENSO variability is defined as the change in frequency and spatial structure of interannual (2–7 years) tropical Pacific variability.

Given the coupled nature of tropical variability, and the sparsity of ocean data, it may not be possible to answer these questions from observations alone. On the other hand, to answer these questions in a modeling study requires a modeling strategy that clearly isolates STC-forced tropical variability. In addition, locally forced mechanisms can generate tropical decadal and ENSO variability, such as, nonlinearities in ocean–atmosphere coupling within the tropics (e.g., Timmermann and Jin 2002) and ENSO-like ocean-to-atmosphere positive feedback with time-delayed negative feedback provided by subtropical Rossby waves (e.g., Knutson and Manabe 1998; Yukimoto et al. 2000). Therefore, it is necessary to determine the significance of STC-forced tropical variability relative to variability forced through atmospheric teleconnections from the extratropics and variability due to intrinsic tropical processes.

In this study we address these questions with the use of a coupled model, comparing completely coupled solutions with solutions that only allow coupling in the tropics while wind stress and heat fluxes outside the tropics are externally specified. We find that there are two distinct signals forced in the North Pacific that can impact the tropics through ocean pathways. This study extends the studies of the impact of North Pacific atmospheric variability on North Pacific Ocean thermocline variability in ocean models, such as Thompson and Ladd (2004) and Liu (1999), to a system that is coupled in the tropics. Among other things, we find that allowing extratropically forced tropical variability shifts primarily 2-year ENSO variability in a tropics-alone simulation to a more realistic broad range of 2–6 years.

This work is part of a hierarchy of model studies designed to investigate the extratropical forcing of the tropical Pacific through ocean pathways. In this study we extend the results of Solomon et al. (2003), obtained using an intermediate coupled system, to a system that utilizes a state-of-the-art AGCM and includes seasonal variability. The next step in this hierarchy of model studies is to investigate the robustness of our findings in a coupled system that includes an ocean GCM.

In Sect. 2 we describe the coupled model and the experimental design used in this study. In Sect. 3 we compare the climate mean and ENSO variability of the control integration to observations. In Sect. 4 we describe the model solution that allows coupling in the tropics and forces the extratropical ocean and atmosphere with climatological mean fields. In Sect. 5 we use an ensemble of model runs forced with output from the control integration in the North Pacific while the tropics are coupled, to assess to what extent the differences between the control and tropics-alone solutions are due to variability forced from the North Pacific. In Sect. 6 we summarize and discuss the findings of this study.

2 Model and experiment design

2.1 The coupled model

The coupled model used in this study is a limited domain 4.5-layer reduced gravity Pacific Ocean model that is anomaly-coupled to the global NCAR CAM3 (Collins et al. 2005) (Coupled Pacific Ocean Global Atmosphere model, hereafter referred to as CPOGA). CAM3 uses bulk formulae to calculate the surface wind stress and heat flux anomalies that force the ocean model. In addition, surface wind speed anomalies are passed into the ocean model's mixed layer subroutine. The ocean model extends from 50°S to 60°N and is run at 1° × 0.5° resolution in the longitudinal and latitudinal directions. The ocean model is nested into the atmospheric model by updating SSTs daily in the Pacific basin with output from the ocean model while monthly mean climatological SSTs (interpolated to daily values) are prescribed elsewhere. The climatological SSTs are a composite of the annual cycle for the period 1950–2001, using the global HadISST OI dataset prior to 1981 and the Smith/Reynolds EOF dataset post-1981. A land surface model calculates fields over land (the NCAR CLM2). The atmospheric model is run at T42 resolution (approximately 2.8° × 2.8°) with 26 vertical levels.

The ocean model is based on the 3.5-layer reduced gravity Pacific Ocean model used in Kleeman et al. (1999) and Solomon et al. (2003). The additional layer in the current model allows for the simulation of both a permanent and seasonal thermocline in the extratropics and an upper and lower thermocline in the Tropics. In addition, the mixed layer physics in the model is parameterized using a Kraus–Turner bulk mixed layer model (Kraus and Turner 1967). The adequacy of this parameterization in simulating the mixed layer temperature of a large eddy simulation model was demonstrated by Wang (2003). The ocean model is modified in this way to allow it to be able to simulate the observed seasonal variation of extratropical subduction.

Four active layers overlie a deep, inert layer of 0°C temperature where the pressure gradient field is assumed to vanish. Each of the layers corresponds primarily to a single water mass type, namely, mixed layer water (T1), upper-thermocline water (T2), lower-thermocline water (T3), upper-intermediate water (T4) in layers-1, -2, -3, and -4, respectively. These layers have thicknesses; H1, H2, H3, and H4.

A mean inflow of 10 Sv (1 Sv = 10^6 m^3 s^{-1}) in layer-4 in the southwest corner of the basin and a compensating outflow of 10 Sv divided evenly among layers-1 through layer-3 at the western boundary between 4°N–8°N are included to incorporate the Indonesian Throughflow. The throughflow is required to produce mean transport

pathways where intermediate water enters the South Pacific from the Southern Ocean, crosses the equator, and exits the basin in the Indonesian throughflow. Additional details on the ocean model are provided in Solomon et al. (2003).

2.2 Experiment design

The ocean model is spun-up by integrating for 100 years with forcing calculated with observed monthly mean fields. The CPOGA is "anomaly-coupled" such that the ocean passes SST anomalies relative to the ocean model's monthly climate mean from the spin-up run to the atmosphere, which is then added to observed monthly climate mean SSTs. Fields that drive the ocean model are similarly anomaly-corrected.

We isolate STC-forced tropical variability by experiment design, i.e., full atmosphere–ocean interaction is allowed in specific regions. One such strategy was employed by Wu et al. (2003), which they refer to as "partial blocking". Figure 1a illustrates the difference between the model strategy of Wu et al. and the strategy employed in this paper. Partial blocking was accomplished by adding artificial sponge walls in the Pacific Ocean between 15–25°N and 15–25°S where temperature, salinity, and ocean currents were restored toward the annual cycle of the control integration. This strategy is very useful for eliminating STC-forced tropical variability.

We are, however, interested in isolating the impact of STC variability on tropical variability. This is accomplished by limiting the region where the atmosphere forces the ocean. We limit the anomalous atmospheric forcing of the ocean by using a "forcing" strategy in our experiment designs. Forcing means the output of monthly surface air temperature and wind anomalies from the control integration (CNT, described in Sect. 3) are used to calculate surface heat flux and wind stress in limited regions. This is similar to the "partial coupling" strategy used by Wu et al. (2003). In their strategy, however, atmospheric anomalies from the coupled model are used to calculate surface heat flux and wind stress, allowing only atmospheric variability due to coupling in the extratropics and internal variability to force the ocean. We use output from the control integration instead of allowing limited extratropical regions to be coupled in order to include the influence of atmospheric teleconnections from the Tropics on surface atmosphere anomalies.

We use a "masking" strategy to limit the region where the ocean forces the atmosphere. Masking in this case mean that SST anomalies are set to zero. In this way we can both specify the forcing of the extratropical oceans and investigate how this forcing impacts climate globally through atmospheric teleconnections from the tropics.

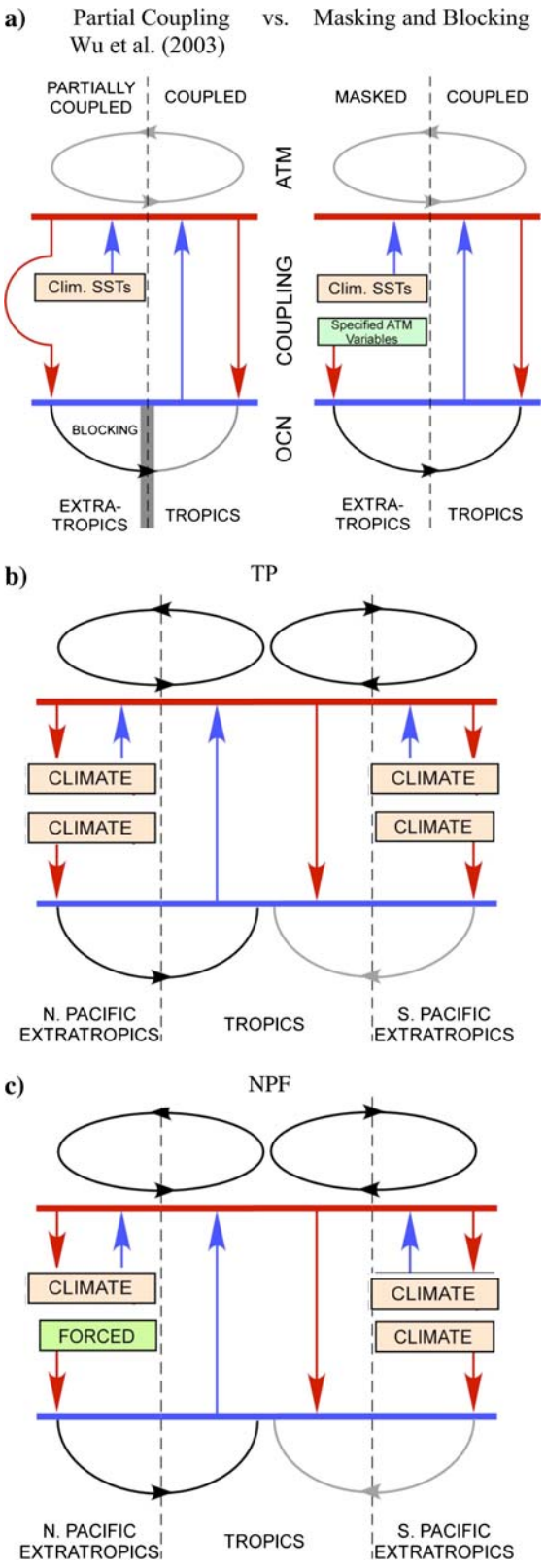

Figure 1b, c are schematic diagrams of the two model configurations beside CNT that are discussed this paper. The tropics-alone configuration (referred to as TP from

◀ **Fig. 1** **a** Schematic of modeling strategy used by Wu et al. (2003) (*left*) compared to the modeling strategy used in the proposed research (*right*). **b** Model configuration designed to limit forcing to the Tropical Pacific Ocean (*TP*). **c** Model configuration designed to limit forcing to the North Pacific Ocean while the tropical Pacific is coupled (*NPF*). The schematics are divided vertically into three sections; the atmosphere, air–sea coupler, and the ocean, and horizontally in two sections to show the different treatment of the tropical and extratropical Pacific Ocean. The *red arrows* are used to indicate how the atmospheric forcing of the ocean is configured. The *blue arrows* are used to indicate how the ocean's forcing of the atmosphere is configured. *Arrows* that begin at the ocean or atmosphere are used to indicate that anomalies from this model are passed to the other model unchanged. *Gray lines* in the atmosphere are used to indicate that atmospheric teleconnections from the extratropical Pacific Ocean to the tropical Pacific Ocean have been suppressed. *Gray lines* in the ocean are used to indicate that oceanic teleconnections from the extratropical atmosphere to the tropical Pacific Ocean have been suppressed

hereafter, shown in Fig. 1b) masks both ocean and atmosphere anomalies, as described above, poleward of 18°. The North Pacific configuration (referred to as NPF hereafter, shown in Fig. 1c) is forced by wind stress and heat fluxes output from CNT, as described above, while the ocean-to-atmosphere fluxes poleward of 18°N and S are computed using climatological SSTs. In this configuration the tropics are coupled. Edge effects are reduced by linearly smoothing the heat flux and wind stress that force the ocean model and the SSTs that force the atmospheric model at 18°N and 18°S on the atmospheric grid.

3 Simulated climatology and ENSO

In this section we compare the climate mean and ENSO variability of the control integration to observations. In the control (CNT) integration, SST anomalies are passed from the ocean to the atmosphere and wind stress, wind speed, and heat flux anomalies are passed from the atmosphere to the ocean from 50°S to 60°N.

3.1 Mean state

In Fig. 2a, b we compare the climatological annual mean skin temperature from CNT with the Hadley Center SST climatology (Rayner et al. 2003; hereafter referred to as HADISST). As expected from the anomaly-coupled design, there is a close correspondence between the model's skin temperature and observations. This indicates that the model's climate drift is negligible. In addition, displacement of the westward extent of the climate mean cold

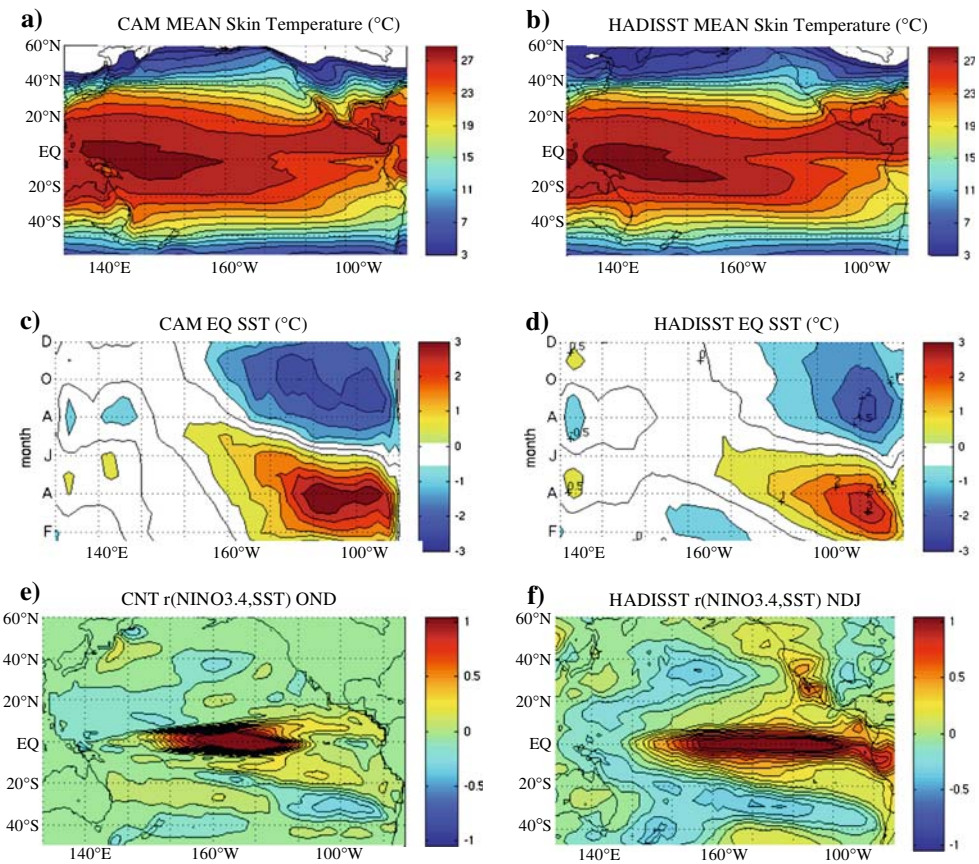

Fig. 2 Climatological annual mean skin temperature from CNT (**a**) compared to the HadISST climatology (**b**), in units of °C. The seasonal cycle of equatorial SSTs (minus the annual mean) from the control integration (**c**) and observations (**d**), in units of °C. Regression at zero lag between (**e**) HadISST NDJ NINO3.4 with NDJ SSTs. (**f**) CNT OND NINO3.4 with OND SSTs. CNT. **a**, **b** CI = 2; **c**, **d** CI = 0.5; **e**, **f** CI = 0.1)

tongue from the central Pacific to the western ocean, a common problem in fully-coupled climate models, is not seen in our simulation. Fully coupled climate models also have difficulty simulating the observed seasonal cycle of equatorial SSTs, which can disrupt the observed phase-locking of ENSO variability (Joseph and Nigam 2005). Comparing the seasonal cycle of equatorial SSTs in the model to observations shows that this bias is not found in the CNT solution (Fig. 2c, d).

The seasonal cycle of the mixed layer depth is well simulated in CPOGA, which is critical for adequately simulating the location and timing of extratropical subduction. Note that model mixed layer depths are deeper in regions where T1 is approximately equal to T2, due to the coarse resolution of the ocean model. It is during the end of winter/beginning of spring that a rapidly shallowing mixed layer causes water to be irreversibly mixed downward and laterally into the permanent thermocline.

3.2 Subsurface transports

Four active layers allows for the simulation of both the tropical cell, where water recirculates within the tropics in layers-1 and -2, and the subtropical cell, where water of extratropical origin flows to the equatorial thermocline in layers-2 and -3. To compare the model's transports with observations we calculated observed meridional transports integrated over the depth of layers-2 and -3 using monthly mean 1980–2004 NOAA Pacific Hindcast data (Behringer et al. 1998). Meridional transport in layer-2 from the model (Fig. 3a) and observations (Fig. 3c) shows the equatorward transport of water within 5° of the equator, the lower branch of the tropical cell. Meridional transport in layer-3 in the model (Fig. 3b) compared to observations (Fig. 3d) indicates that subtropical water is transported to the tropics from both the north and south Pacific. Note the poleward transport in the eastern subtropical North Pacific in both CNT and observations where transport of water to the equator through an interior pathway is blocked by the "potential vorticity barrier" (Lu and McCreary 1995).

3.3 ENSO variability and its teleconnections

In Fig. 2e, f we plot the spatial structure of ENSO and its teleconnections patterns from CNT (HADISST) by regressing OND (NDJ) SSTs to OND (NDJ) NINO3.4 SST anomalies. OND anomalies are plotted for the CNT integration since ENSO events in the model tend to peak 1–2 months earlier than observed events. However, the springtime barrier, when weak SST anomalies cause a decrease in predictability, is well simulated (figure not shown). The model solution is seen to have variability of similar magnitude to observations. The model solution also has a realistic westward extent of positive SST anomalies, meridional extent of equatorial SST anomalies, and structures of off-equatorial and extratropical negative SST anomalies. On the other hand, the equatorial SST anomalies do not extend to the eastern boundary as observed and the SST anomalies along the North American coast are weak. All runs done with this model have an ENSO structure similar to Fig. 2e.

In Fig. 4a, b we plot the power spectra of monthly NINO3.4 (150–90°W, 5°S–5°N) SST anomalies from observations and the CNT model solution, respectively

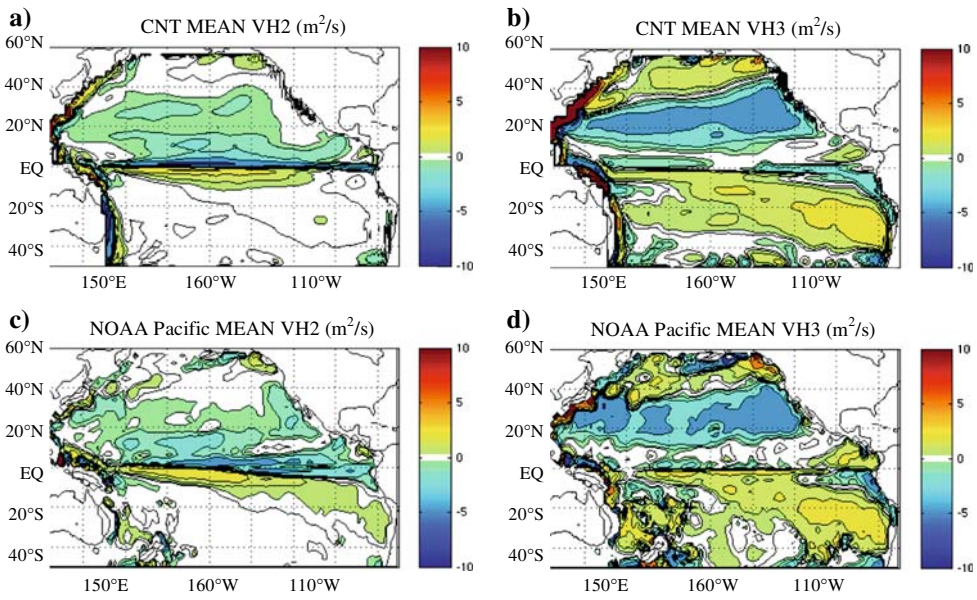

Fig. 3 Climatological annual mean meridional transport in the seasonal thermocline (**a**) and permanent thermocline (**b**) from CNT compared to the NOAA Pacific hindcast (**c**, **d**), in units of m^2/s. (contours = ± 0.25, 0.5, 1, 2, 5, 10)

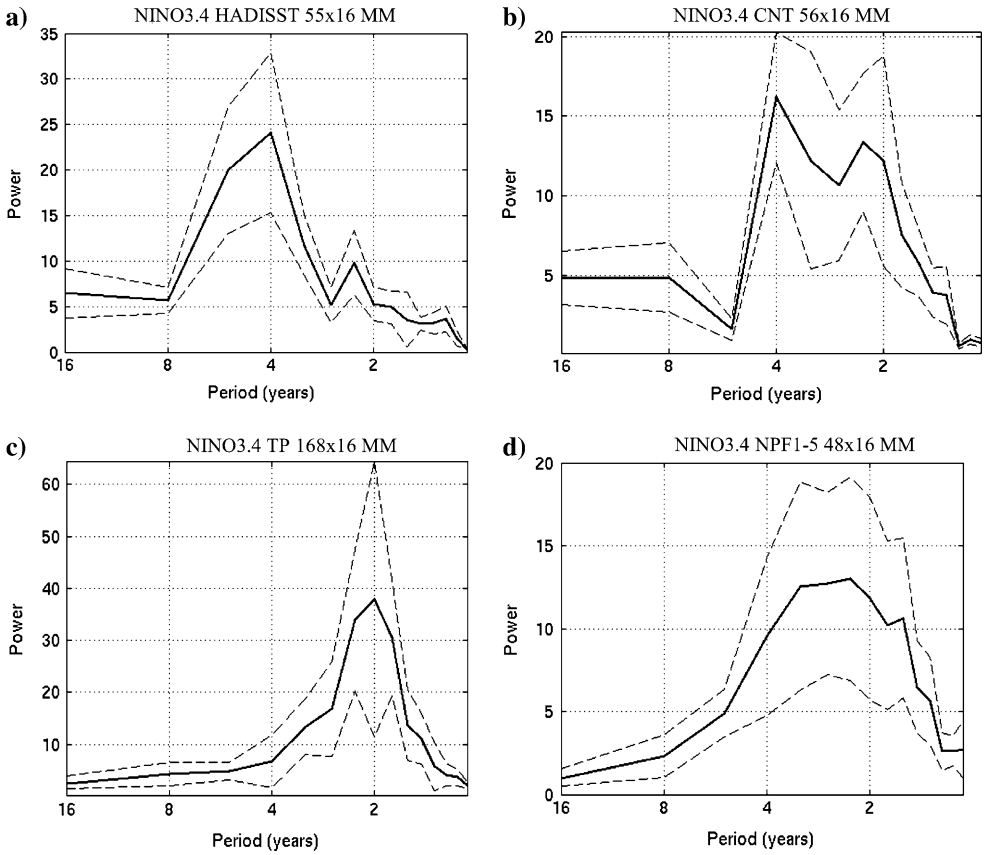

Fig. 4 Spectra of NINO3.4 SSTs. Time series analysis is performed on 16-year chunks of monthly mean data. Mean and one standard deviation are indicated by *solid* and *dashed lines*. **a** HadISST. **b** CNT. **c** TP. **d** NPF1-5

(note scales are different). Spectral analysis is performed on 16-year chunks from each time series. The solid line in each figure shows the mean of the spectra, the dashed lines indicate one standard deviation. Variability on a broad range of timescales is seen in both figures, although the simulations tend to have too much power in the 2-year timescale relative to observations. Also, average power at a period of 4 years in the model solution is approximately 50% smaller than observed.

4 Tropical variability generated locally within the tropics

In order to understand the significance of tropical variability forced from the North Pacific it is necessary to know how large this variability is relative to tropical variability forced locally within the Tropics. We find that ENSO variability in the tropics-alone simulation (TP) is significantly different from ENSO variability in the control simulation. First, when extratropical variability is excluded, ENSO variability becomes sharply peaked at a 2-year period (Fig. 4c). Comparing Fig. 4b, c it is seen that limiting the coupling to the tropics also reduces tropical decadal variability. In the next section we will identify to what extent these differences are due to tropical variability forced from the North Pacific.

Both tropical and extratropical wind forcing contribute to tropical transport variability in the permanent thermocline. To identify this variability generated within the tropics, we plot correlations between zonal wind stress zonally-averaged across the basin (TXZM) and variability in the upper, lower and equatorial branches of the North Pacific STC using output from TP (Fig. 5). We chose meridional transports in the surface layer (VH1ZM) and meridional transports in the permanent thermocline (VH3ZM) at 9°N zonally-averaged across the basin as indicators of variability in the upper and lower branches to be consistent with previous modeling and observational studies of Pacific STC variability. An indicator of variability in the equatorial branch of the STC is mean upwelling between layers-2 and -3 (W2EQ). The relationship between VH3ZM variability and equatorial SSTs is plotted in (Fig. 5d).

Looking at the correlations between VH1ZM anomalies at 9°N and TXZM anomalies first (Fig. 5a), the largest correlations are found at zero lag, with negative correlations centered at 9°N and positive correlations at the equator. For the subsurface branch, negative correlations between VH3ZM anomalies at 9°N and TXZM anomalies

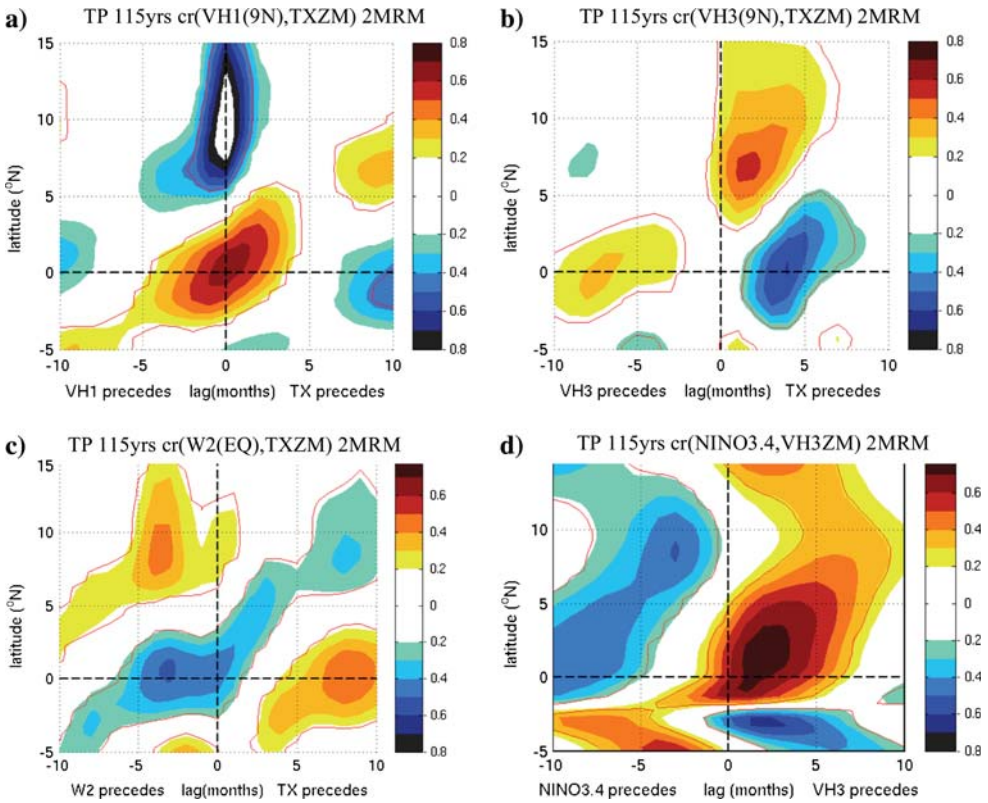

Fig. 5 Lag correlations from tropics-alone integration as a function of latitude and smoothed with a 2-month running mean. **a** Correlations between mean meridional transports in the surface layer at 9°N and zonal mean zonal wind stress as a function of latitude. **b** Correlations between mean meridional transports in the permanent thermocline at 9°N and zonal mean zonal wind stress as a function of latitude. **c** Correlations between mean upwelling from layer-3 to layer-2 at the equator and zonal mean zonal wind stress as a function of latitude. **d** Correlations between NINO3.4 SSTs and zonal mean meridional transports in the permanent thermocline (VH3ZM). Only correlations that exceed the 95% significance levels are shown. The *red contour line* indicates correlations with greater than 99% significance. CI = 0.1

are a maximum at the equator when the wind stress precedes the transports by 4 months (Fig. 5b). For the equatorial branch, a decrease in upwelling at the equator precedes an increase in TXZM at the equator by 3 months (Fig. 5c). In addition, a decrease in upwelling at the equator is associated with a decrease in TXZM at 9°N, as is typically observed during an El Niño event. These results together illustrate a change in the strength of the North Pacific overturning circulation within the Tropics by tropical dynamics alone (i.e., not involving changes in subtropical subduction). This variability is equivalent to the recharge and discharge of mass off and on the equator that occurs during an ENSO cycle, as described by Jin (1997), extended to the edge of the tropics. This tropically forced overturning circulation variability impacts NINO3.4 SSTs 6 months after the VH3ZM anomalies at 9°N (Fig. 5d).

5 Tropical variability forced from the North Pacific

In order to determine whether the broadening of the NINO3.4 power spectra from the control integration relative to the tropics-alone integration is due to forcing from the extratropical North Pacific, we designed a series of model runs that isolate the extratropical signal from the tropical variability ("noise") generated in the tropics. In these model runs we specify the forcing of the North Pacific Ocean (NPF) while allowing the tropics to be coupled. In this series of runs we force the North Pacific Ocean (north of 18°N) with 49-years of monthly mean wind stress and heat fluxes output from CNT, while the North Pacific atmosphere is forced by climatological SSTs and no anomalies are passed between the South Pacific Ocean and atmosphere. The extratropical North Pacific atmospheric forcing is repeated five times while the ocean and atmosphere from the AGCM is continuously integrated. This allows for a continuous 245-year integration in the tropics.

In Fig. 4d we plot the power spectra of NINO3.4 SSTs from the five individual NPF ensemble members (hereafter referred to as NPF1–5). Comparing this figure to Fig. 4c it is clearly seen that forcing from the North Pacific broadens the sharp 2-year spectral peak in the tropics-alone integration, similar to the spectra from the CNT integration (Fig. 4b). It is interesting to note that the enhanced decadal variability in CNT relative to TP is not systematically seen in the NPF runs. This is an indication that the decadal variability in CNT may be forced by STC pathways from the South Pacific or through the atmosphere.

5.1 Structure of North Pacific variability that forces tropical variability

In order to isolate the systematic forcing of the tropical Pacific from the North Pacific we averaged the five NPF

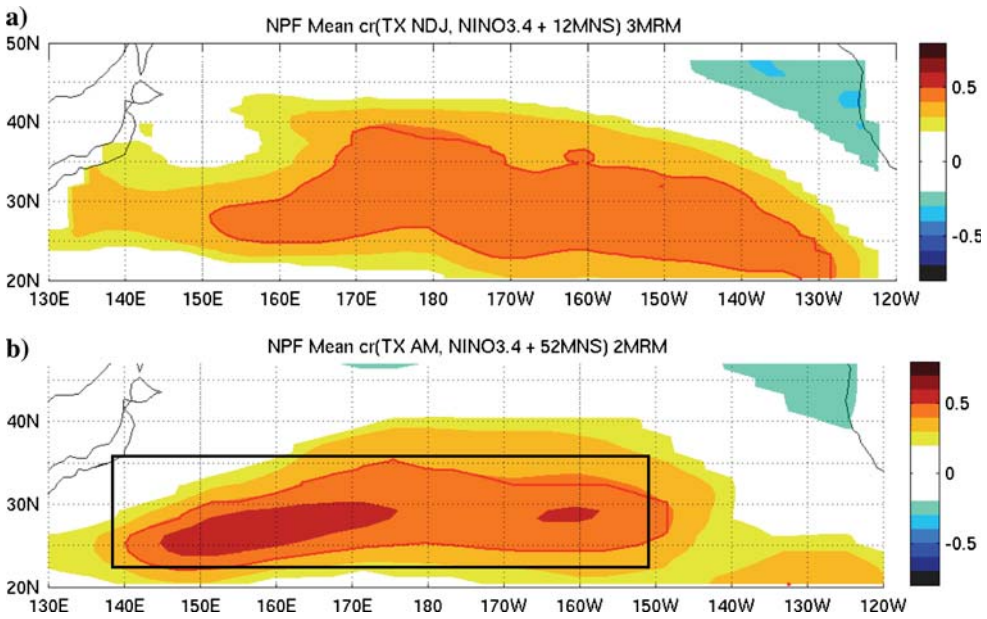

Fig. 6 NPF ensemble mean zonal wind stress correlated with NINO3.4 SSTs. **a** NDJ zonal wind stress correlated with NINO3.4 SSTs 12 months later. All data is smoothed with a 3-month running mean. **b** April–May zonal wind stress correlated with NINO3.4 SSTs 52 months later. All data is smoothed with a 2-month running mean. Only correlations greater than 90% are contoured. Ninety-nine percent significance levels are denoted with a *red contour line*. The TX(WNP) region (140°E–150°W, 22–36°N) is indicated with a *black box*

ensemble members to form an ensemble mean. We trace the feedbacks from the North Pacific to the Equator by first performing a series of lag correlations between NINO3.4 SSTs and zonal wind stress in the extratropical North Pacific.

With the lag correlations we were able to identify two signals from the North Pacific to the Tropics—a relatively fast signal when the extratropical variability precedes tropical variability by 10–12 months and a relatively slow signal when extratropical variability precedes tropical variability by approximately 52 months. In Fig. 6 we plot the spatial pattern of the extratropical zonal wind stress for these two signals. Unless otherwise stated, only correlations greater than 90% are plotted and 99% significant correlations are indicated with a red contour line. We use the Student's *t* test to calculate the statistical significance of correlations discussed in this paper. Effective degrees of freedom are calculated following Livezey and Chen (1983). Both patterns extend across the basin with the slow signal having larger correlations equatorward of 25°N and west of the dateline while the fast signal has significant correlations up to 30°N that extend into the eastern Pacific. The black box in the figure outlines the area averaged to form an index of zonal wind stress [referred to hereafter as TX(WNP)]. Figure 7 shows that the power spectra of zonal wind stress averaged in the TX(WNP) region. This figure shows that atmospheric variability in this region is forcing the ocean within the 2–6 year period range.

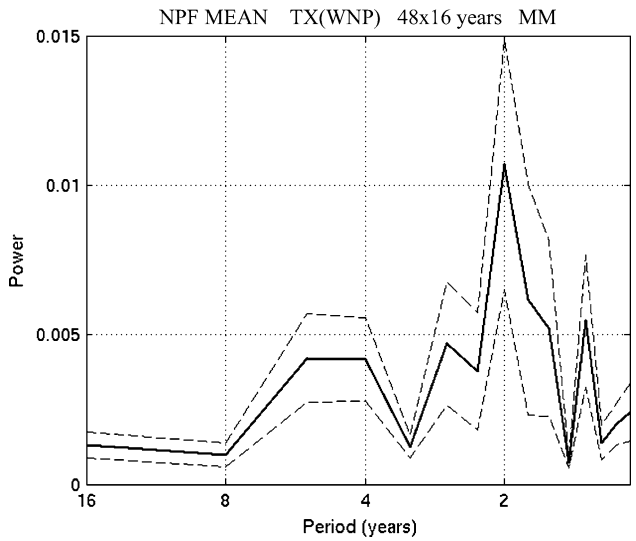

Fig. 7 NPF ensemble mean spectra of zonal wind stress anomalies in the TX(WNP) (140°E–150°W, 22–36°N) region. Time series analysis is performed on 16-year chunks of monthly mean data. Mean and one standard deviation are indicated by *solid and dashed lines*

In Fig. 8 we plot the correlations between NINO3.4 SSTs and zonal wind stress averaged in the TX(WNP) region (outlined in Fig. 6). This figure shows the correlations for zonal wind stress on a given month with tropical SSTs at a given lag. Only 95% significant correlations are shown. Two broad regions of significant correlations are seen (marked with dashed circles). The first region is seen where positive correlations for wind stress forcing from November to May lead tropical SSTs by 10–12 months—the fast signal. The second region is seen where springtime wind stress forcing leads tropical SSTs by 50–55 months—the slow signal.

To show that this tropical signal is robust we plot the mean and mean divided by the standard deviation of the NINO3.4 SST anomalies from the five NPF ensemble members in Fig. 9. In this figure it is seen that almost all of the peaks in tropical SSTs (magnitudes greater than

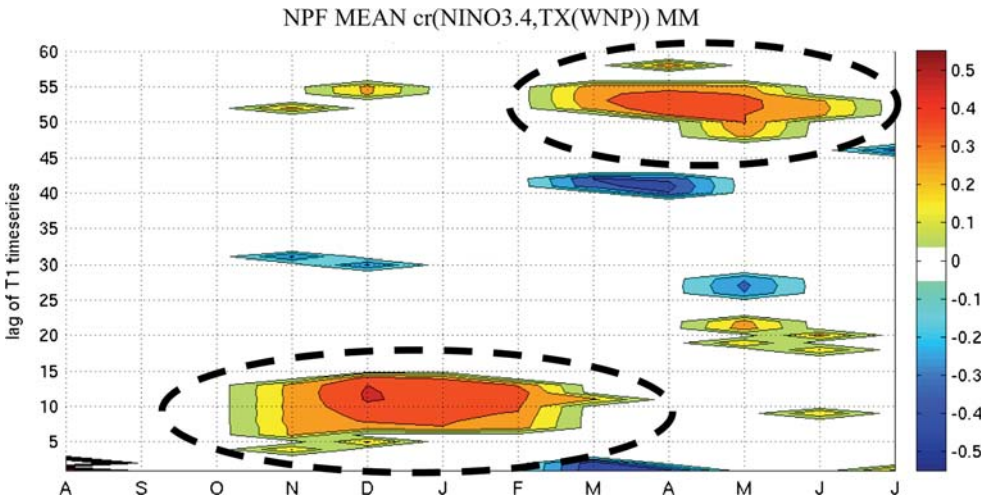

Fig. 8 Correlations between zonal wind stress forcing, averaged in the region of (140°E–150°W, 22–36°N), and NINO3.4 SSTs, as a function of the month of the forcing and the lag of the SSTs. The fast and slow signals discussed in the text are marked with *dashed black circles*. Only correlations greater than 95% are plotted

0.25°C) have an absolute value of (mean/STD) greater than 0.5, an indication that the tropical response to the extra-tropical forcing is robust among the ensemble members.

Based on previous studies (e.g., Thompson and Ladd 2004) of long oceanic Rossby waves forced in the sub-tropical North Pacific, our working hypothesis is that the fast signal is a first-mode baroclinic Rossby wave forced by Ekman pumping and the slow signal is a higher-order mode baroclinic Rossby wave forced by end of winter/beginning of spring subduction. To this end it is informative to look at the climatic-mean April–May subduction (W2) and wind stress (TX, TY) in the subtropical North Pacific (shown in Fig. 10a, b). W2 is the exchange of mass between the seasonal mixed layer and the permanent thermocline and it therefore a measure of subduction. The dashed red contours in Fig. 10a indicate springtime outcropping lines for the 24.2, 24.5, 24.8, 25.1 isopycnals (from south to north respectively). We focus on the 24.5–25.1 isopycnal range because these are the isopycnals that intersect the core of the equatorial undercurrent, shown in Fig. 10c. Subduction is a maximum at the end of winter/beginning of spring in the model as in observations (results not shown). It is seen in Fig. 10a that the 24.5–25.1 isopycnals outcrop in the region of climate mean springtime subduction from 170°W to the western boundary. North of the dashed red lines, water that subducts flows to the equator below the core of the equatorial undercurrent.

In Fig. 11 we plot the correlations between May subduction anomalies and NINO3.4 SSTs 52 months later (Fig. 11a) and April–May surface heat flux anomalies and NINO3.4 SSTs 52 months later (Fig. 11b). In Fig. 11a, May subduction anomalies are used instead of April–May anomalies because this month is when the W2 anomalies are largest. In Fig. 11a, the region of greater than 99% significant correlations (indicated by the red contour) lies within the region of maximum springtime subduction

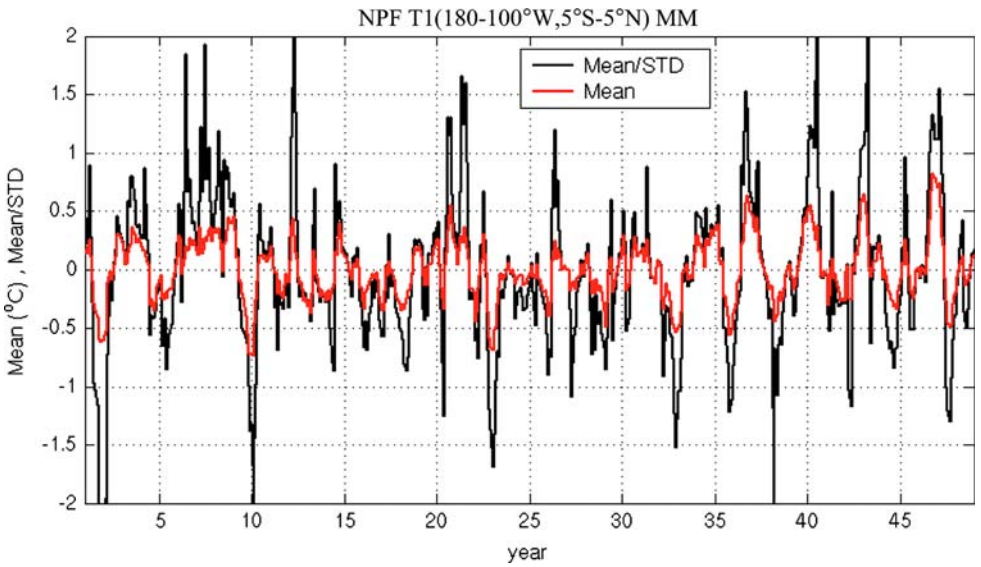

Fig. 9 Time series of monthly mean tropical east Pacific SSTs from the five NPF ensemble members, in units of °C. The ensemble mean in *red* and the mean divided by the standard deviation in *black*

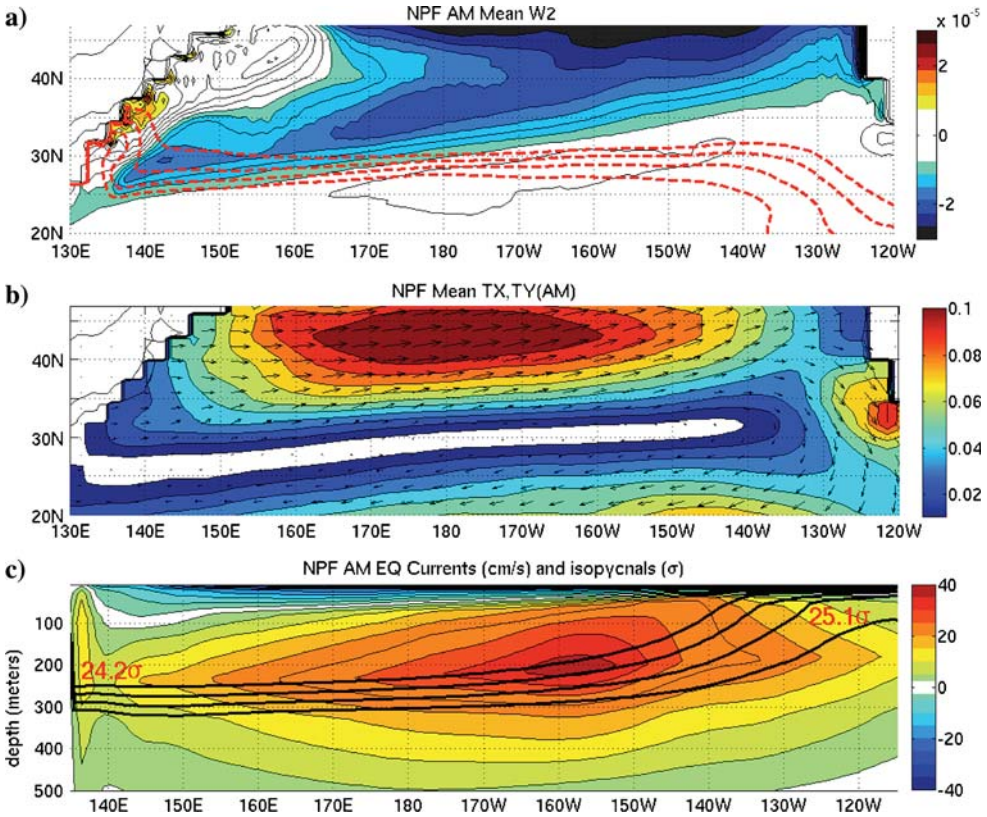

Fig. 10 **a** NPF ensemble mean April–May W2, in units of ms^{-1}. Isopycnals 24.2, 24.5, 24.8, 25.1σ are shown with *red dashed lines*. CI = 3 × 10^{-6}. **b** NPF ensemble mean April–May magnitude and vector wind stress, in units of Nm^{-2}. CI = 0.01. **c** NPF ensemble mean April–May equatorial currents, in units of cm s^{-1}. Isopycnals 24.2, 24.5, 24.8, and 25.1σ are overlaid with *thick black contours*. CI = 5

(Fig. 10a) and overlaps with the 24.5–25.1 isopycnal outcropping in the western Pacific. This anomalous subduction is forced by heat flux anomalies (Fig. 11b), since Ekman pumping anomalies are small in this region (results not shown). The cooling in Fig. 11b is associated with an increase in the eastward zonal wind stress (Figs. 6b, 10b) and the heating is associated with a decrease in the westward zonal wind stress. In addition, the lack of significant correlations with sea level height anomalies in the North Pacific at this lag are an additional indication that this signal is a "buoyancy-induced" higher-order baroclinic Rossby wave.

5.2 Pathways to the tropics

By contrast, correlations between NINO3.4 SSTs anomalies and wintertime sea level height anomalies 12 months

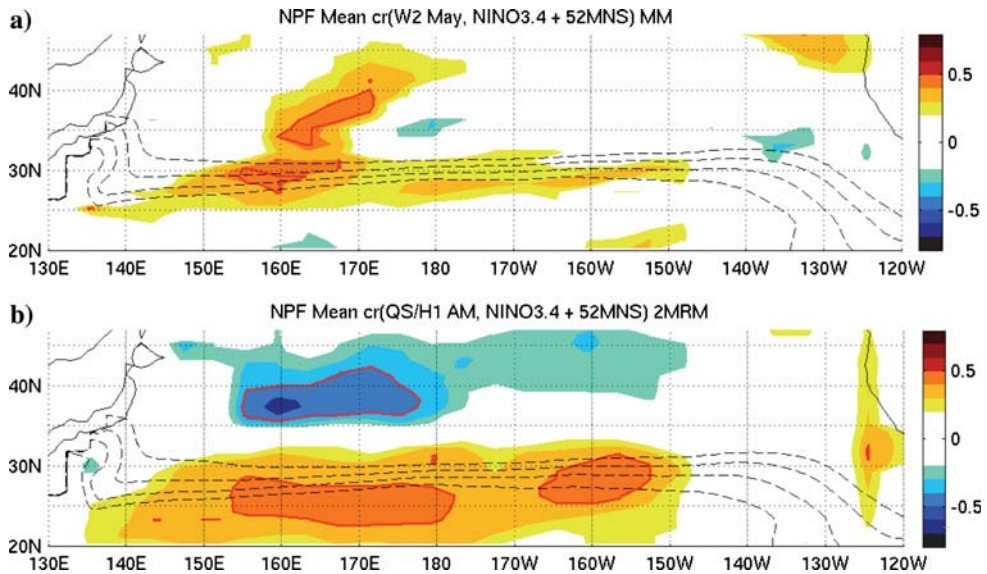

Fig. 11 **a** Correlations between NPF ensemble mean North Pacific May W2 and NINO3.4 SSTs 52 months later. *Dashed black lines* indicate May mean isopycnals 24.2, 24.5, 24.8, 25.1σ. CI = 0.1. **b** Correlations between NPF ensemble mean North Pacific April–May QS/H1 and NINO3.4 SSTs 52 months later. *Dashed black lines* indicate April–May mean isopycnals 24.2, 24.5, 24.8, 25.1σ. CI = 0.1. Only correlations greater than 90% are shown. Ninety-nine percent significance levels are denoted with a *red contour line*

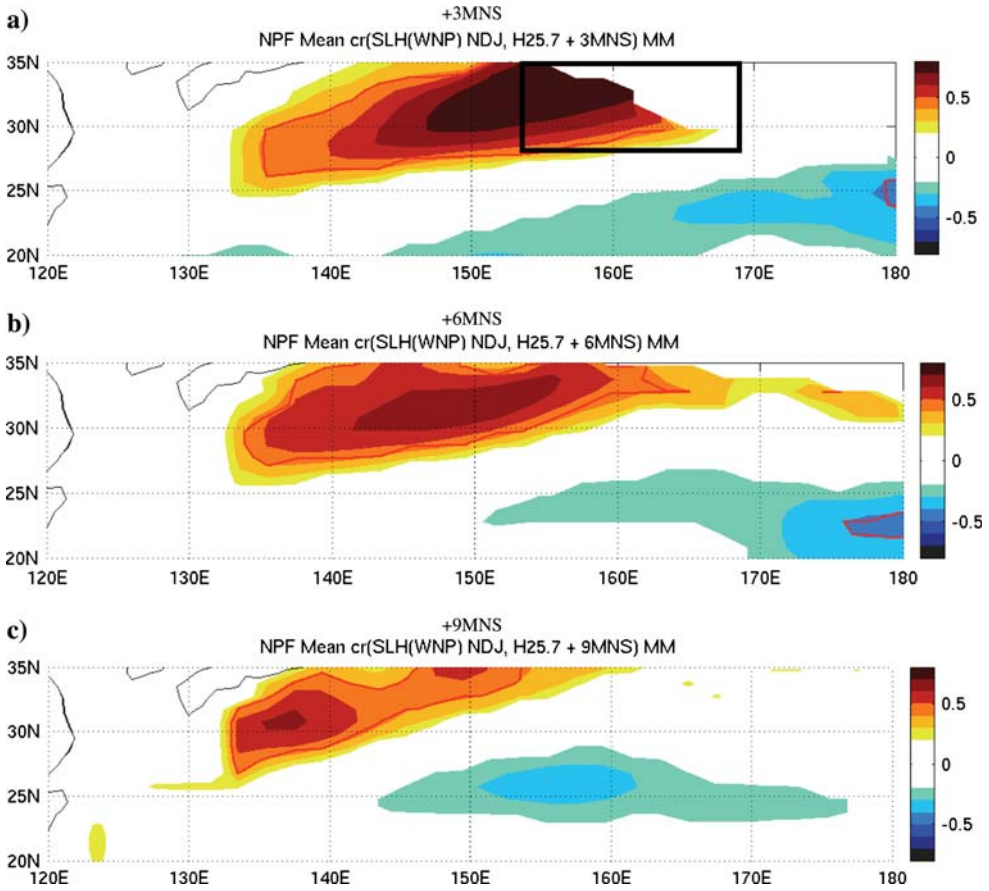

Fig. 12 Correlations between monthly mean SLH (WNP) and H on the 25.7σ isopycnal in the North Pacific. SLH(WNP) is marked with a *black box* in a. CI = 0.1. **a** H follows by 3 months. **b** H follows by 6 months. **c** H follows by 9 months. Only correlations greater than 90% are shown. Ninety-nine percent significance levels are denoted with a *red contour line*

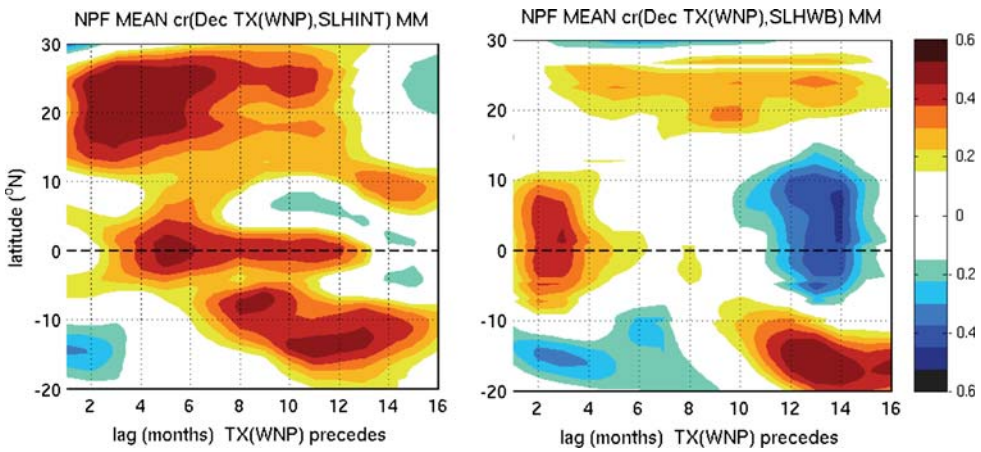

Fig. 13 The pathway of the fast signal from the region of subtropical forcing to the equator. Correlations between December zonal wind stress forcing, averaged in the region of (140°E–150°W, 22–36°N), and sea level height zonally integrated in the interior of the basin (*left*) and along the western boundary (*right*), as a function of latitude of the sea level height anomalies and lag. All fields are monthly means. Only correlations greater than 95% are plotted. Ninety-nine percent significance levels are indicated with a *red contour line*

earlier have greater than 99% significant correlations in the western Pacific centered on 32°N, 160°E (results not shown). Interestingly, this is not the region of maximum wintertime mean wind stress or wind stress variability. This result suggests that the location of these significant correlations may be determined by the optimal pathways to the equator and the optimal time lag for triggering tropical variability. An example of a first-mode baroclinic Rossby wave triggered in the region described above (outlined by the black box in Fig. 12a and referred to as SLH(WNP)) is shown in Fig. 12. Note that the longitudes plotted are west of the dateline. This figure shows the correlations between wintertime first baroclinic Rossby wave source, SLH(WNP), and variability of the depth of the 25.7

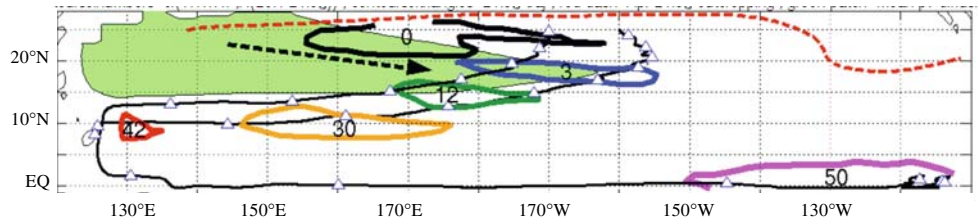

Fig. 14 The pathway of the slow signal from the region of subtropical North Pacific forcing to the equator. The signal starts at the April–May mean 24.5σ outcropping line (*red dash line*), travels eastward along mean potential vorticity contours (the *green shading* shows the May mean 3.5×10^{-10} m^{-1} s^{-1} potential vorticity contour), then follows advective pathways to the equator. The *thick contour lines* show correlations with greater than 95% significance between the H(24.5–25.1σ) anomalies and May TX(WNP) at lags of 0 (*black*), 3 (*blue*), 12 (*green*), 30 (*yellow*), 42 (*red*). The magenta contour shows greater than 95% significant correlations between May TX(WNP) and H(25.7σ) at a 50 month lag. The *two black lines* show trajectories along the 24.8σ isopycnal from the subtropics to the equator with year intervals marked with *triangles*

isopycnal (a measure of the movement of the thermocline and therefore equivalent to sea level height variability) at 3, 6, and 9 months lag (Fig. 12a, b, c, respectively). Propagation is clearly seen from the source to the western boundary within 9 months. It is interesting to note that in Fig. 12a 99% significant correlations extend to 135°E within 3 months of the forcing.

Since the fast signal propagates as a first-mode baroclinic Rossby wave, we isolate the path of this signal to the tropics with sea level height variability. This is seen in Fig. 13 where we correlate December TX(WNP) with sea level height variability zonally averaged in the interior of the basin (Fig. 13a) and along the western boundary (Fig. 13b) as a function of lag and latitude of the sea level height anomalies. Figure 13a shows that these waves in the extratropics propagate within the interior of the basin for 3–9 months then propagate along the western boundary to the equator where the signal then moves along the equator as a Kelvin wave to the eastern boundary. The fast response at the equator is due to the wind stress forcing extending to within 20° of the western boundary.

Since the slow signal propagates as a higher-order mode baroclinic Rossby wave, we isolate the path of this signal to the equator with thickness anomalies between then 24.5σ and 25.1σ isopycnals, a measure of a change in the structure of the thermocline. Figure 14 shows that the pathway starts in the western subtropical Pacific at the 24.5σ outcropping line (red dashed line). The signal propagates eastward along contours of mean potential vorticity (indicated by the green shading) and against the mean currents. After this eastward "diffusion" of the signal it then follows the advective pathway to the equator. We show this in the figure by overlaying trajectories along the 24.8σ isopycnal from the subtropics to the equator with 95% significance contours of the correlation between the May TX(WNP) and H(24.5–25.1σ) at 0, 3, 12, 30, 42, and 50 month lags. The close approximation of the travel time of the signal to the equator with the advection by mean currents is seen by comparing the lags with the triangles along the trajectories that mark 1-year intervals. The contour at the equator correlated with H at 25.7σ to show the impact on the depth of the near-equatorial thermocline.

In order to compare with previous studies of the impact of North Pacific variability on the tropics, we calculated the meridional transports integrated along a latitude circle on 25.4–25.1σ isopycnal surfaces and at the surface as a function of latitude. The poleward surface transports make up the upper branch of the North Pacific STC and the equatorward transports within the thermocline make up the lower branch of the North Pacific STC. We found that the slow signal has no clear signal in zonally integrated meridional transports (results not shown). In addition, we see no clear signal in temperature anomalies along the slow signal pathway. Clearly, this slow signal is different from those identified by Gu and Philander (1997) and Kleeman et al. (1999).

5.3 Response in the tropics

What impact do these two mechanisms have on equatorial dynamics? To gain insight into this question we plot the regression coefficients between NDJ TX(WNP) and tropical SSTs when SSTs follow by 6, 9, 12 and 15 months in Fig. 15. Figure 13 showed that the fast signal gets to the equator within 6 months of the forcing in the subtropics. Figure 15 shows that when this subsurface signal reaches the equator it impacts tropical SSTs, primarily through upwelling anomalies (results not shown). Positive wind stress anomalies in the WNP region precede maximum positive equatorial SST anomalies by 12 months. The standard deviation of TX(WNP) smoothed with a 3-month running mean is 0.0218 Nm^{-2}. Therefore, one standard deviation in TX(WNP) precedes a 0.26°C maximum equatorial SST anomaly 12 months later. The SSTs anomalies persist into the spring session and are insignificant by the summer.

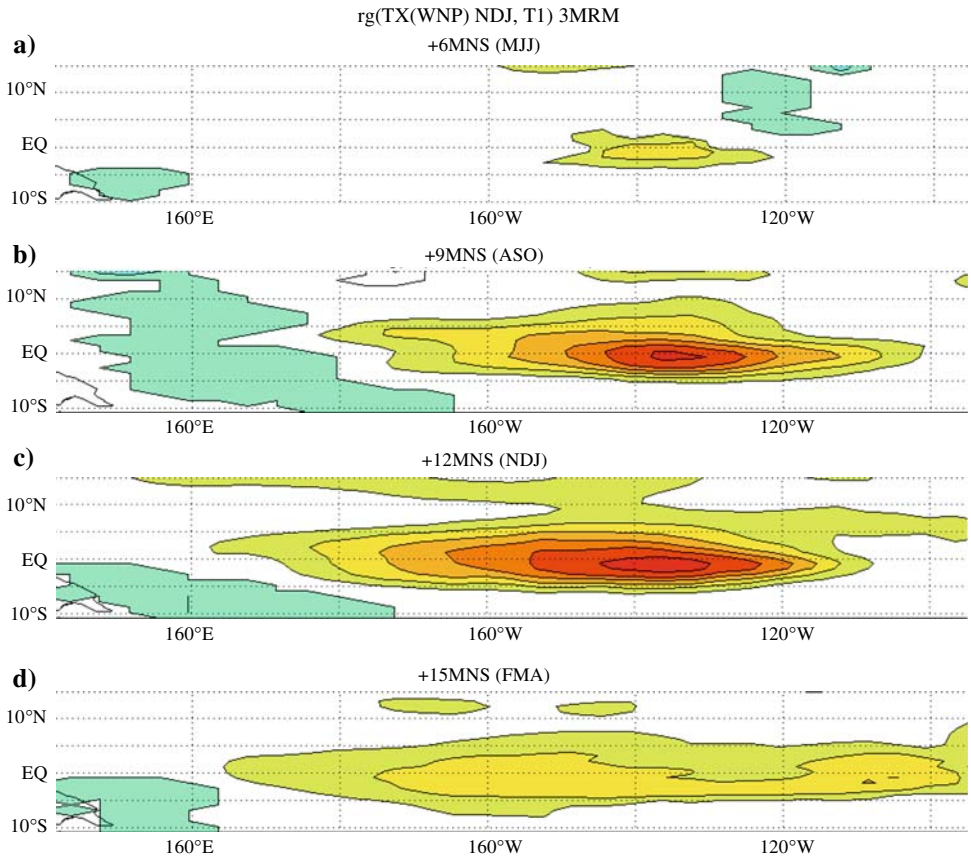

Fig. 15 Regressions between NDJ TX(WNP) and tropical SSTs, in units of °C per N m^{-2}. CI = 2, Max = 12. **a** T1 follows by 6 months. **b** T1 follows by 9 months. **c** T1 follows by 12 months. **d** T1 follows by 15 months. All data is smoothed with a 3-month running mean

In Fig. 16 we plot regressions of April–May TX(WNP) with tropical SSTs at lags of 40, 46, 52, and 58 months. We plot earlier lags to show that significant negative correlations tend to precede the positive correlations by 12 months (as was seen in Fig. 8). Back-correlating tropical SSTs with subduction anomalies 40 and 52 months earlier shows 99% significant correlations in the same region centered on 160–170°E, 30–38°N, indicating that the negative and positive anomalies with a 12 month lag are due to the forcing having a spectral peak at 2 years (Fig. 7). The regression coefficients in Fig. 16 are twice as large as in Fig. 15, indicating that the slow signal is more efficient at forcing tropical SST anomalies than the fast signal. One standard deviation in wind stress forces a tropical SST anomaly with a peak magnitude of 0.52°C 52 months later. Differently from the fast signal, the slow signal forces SST anomalies that peak in fall. These anomalies also persist until spring and decay away by the summer. There is no indication that this signal persists into the following year.

6 Summary and discussion

In this paper we used an anomaly-coupled climate model, and a modeling strategy that specifies wind stress and heat fluxes in the North Pacific with model output from a coupled control integration while allowing the tropics to remain coupled, to demonstrate that atmospheric variability over the North Pacific can impact tropical variability through ocean pathways. We find a fast and a slow signal from the extratropics to the tropics. Both signals are forced by variability within the subtropics (equatorward of 40°N). The fast signal is forced from November to March, while the slow signal is only forced during springtime when buoyancy forcing can effectively trigger higher-order baroclinic modes through subduction anomalies into the permanent thermocline. The fast signal travels as a first-mode baroclinic Rossby wave and triggers tropical variability within a year of forcing. This relatively short lag is due to the wave being triggered within 20° of the western boundary. The slow signal travels as a higher-order mode baroclinic Rossby wave and essentially follows the advective pathway to the equator. The slow signal is found to trigger tropical variability more efficiently than the fast signal with one standard deviation in zonal wind stress forcing tropical SSTs with maximum values of approximately 0.5°C. The slow signal causes pycnocline transport variability that extends from the subtropics to the equator but only impacts surface flow within 10° of the equator, indicating that this variability is occurring on timescales that may be too fast to spin-up a STC. We find that

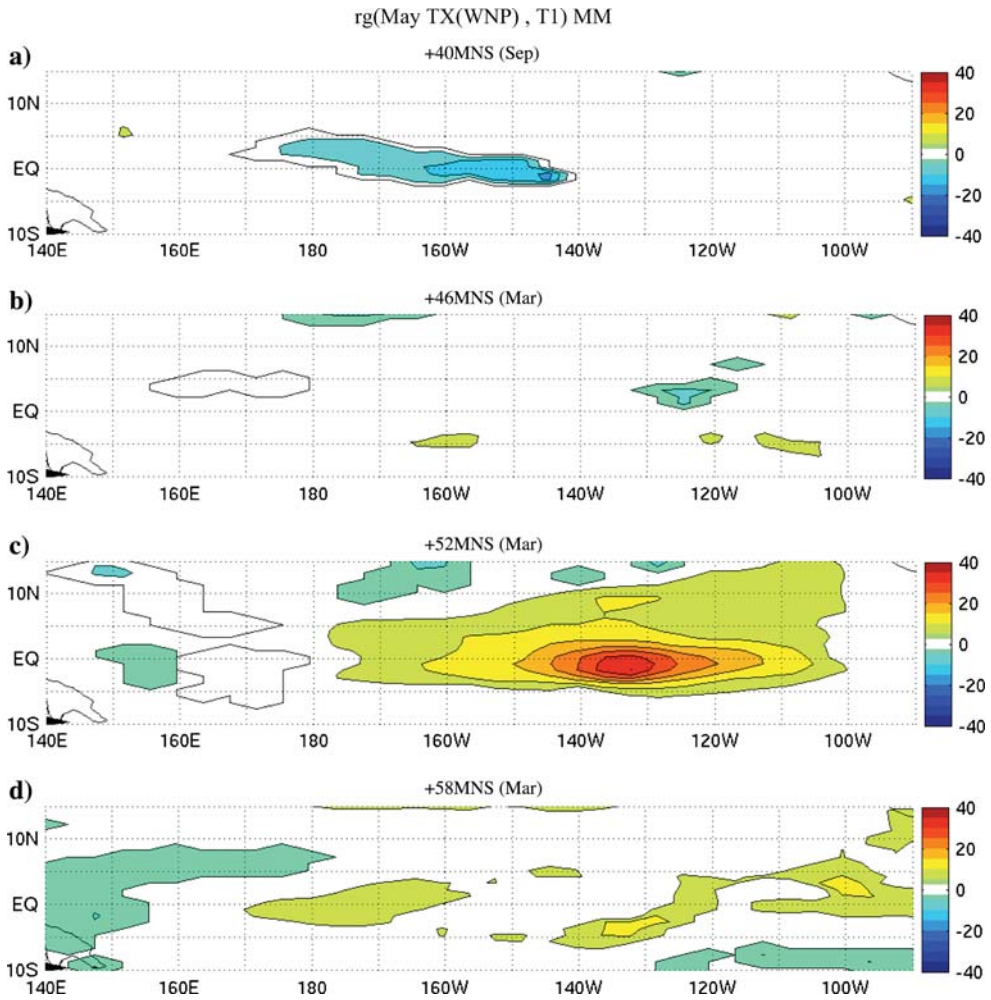

Fig. 16 Regressions between May TX(WNP) and tropical SSTs, in units of °C per N m^{-2}. CI = 4. **a** T1 follows by 40 months. **b** T1 follows by 46 months. **c** T1 follows by 52 months. **d** T1 follows by 58 months

allowing extratropically forced tropical variability shifts a primarily 2-year ENSO period, when all extratropical feedbacks are excluded, to a more realistic broad range of 2–6 years.

The results of this study are essentially an extension of analytic and ocean general circulation model studies of the impact of North Pacific atmospheric variability on North Pacific Ocean thermocline variability, such as Thompson and Ladd (2004) and Liu (1999), to a system that is coupled in the tropics. These studies identify how buoyancy and wind forcing in the extratropics force ocean variability. In this paper, we identified to what extent this variability can impact the tropics. The results of our model studies suggest that a signal generated in the subtropics can reach the equator through ocean pathways and have a significant impact on tropical variability, as was found in previous studies such as Lysne et al. (1997) and Shin and Liu (2000).

Consistent with observational studies that show large interannual variability in the observed STCs within the tropics (McPhaden and Zhang 2002, 2004), we find significant variability in the upper, lower, and equatorial branches of the North Pacific STC associated with coupled tropical feedbacks. However, significant variability in the poleward branch of the STC was not found, indicating that this tropically forced variability is either too fast or too weak to completely spin up the North Pacific STC.

Solomon et al. (2003) found that STC-forced tropical variability from the North Pacific modulates tropical variability on decadal timescales. In our NPF runs, decadal ENSO variability was smaller than in the control integration. The NPF model results indicate that the North Pacific is primarily impacting tropical variability through ocean pathways on interannual timescales, since the winds that force this variability have very little power on decadal timescales. The enhanced decadal variability in the control

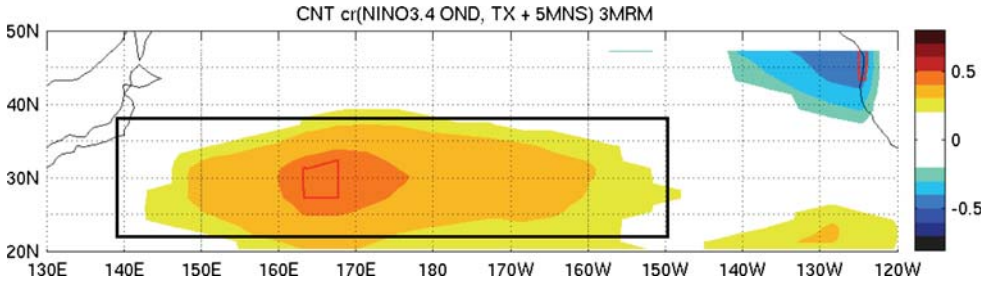

Fig. 17 CNT OND NINO3.4 SSTs correlated with zonal wind stress 5 months later (MAM). All data is smoothed with a 3-month running mean. Only correlations greater than 90% are contoured. Ninety-nine percent significance levels are denoted with a *red contour line*. The TX(WNP) region (140°E–150°W, 22–36°N) is indicated with a *black box*

run may be forced through STC pathways from the South Pacific or from the extratropics through the atmosphere. We are exploring these possibilities in our current research.

An open issue is the nature of processes that cause the slow signal to travel eastward against the mean currents in the first 3 months. This downgradient diffusion is consistent with the studies of Xie et al. (2000) and Shin and Liu (2000). Xie et al. demonstrated that right after the potential vorticity anomaly is subducted into the main thermocline it creates a large density gradient that is quickly diffuses the signal to the southeast. We have shown that, in our study, this downgradient transport follows the low mean potential vorticity tongue from the region of subduction to the southeast into a region where the slow signal is easily advected to the equator by the mean currents.

In this study we find that the optimal region where the extratropical atmosphere can force ocean variability that impacts the tropics is in the central-western subtropical North Pacific. This atmospheric variability forces heat flux, mixed layer depth, and subduction anomalies locally and does not appear to be related to variability in the eastern Pacific that propagates through the ocean to the west, as was found by studies such as Schneider and Miller (2001) and Solomon et al. (2003).

We speculate that the TX(WNP) variability may be due to atmospheric teleconnections from the tropics. In Fig. 17 we plot correlations between OND NINO3.4 SSTs and extratropical zonal wind stress 6 months later (MAM) from the control integration. We again mark the TX(WNP) region with a black box. Clearly, the extratropical variability forced from the tropics is in the region that we found to be most effective in forcing tropical variability. This suggests the possibility that there is a feedback loop between extratropical variability forced by way of the atmospheric bridge from the tropics and tropical variability forced by way of the ocean bridge from the subtropics. This could explain the spectral peaks at 2 and 4–6 years in TX(WNP) seen in Fig. 8. On the other hand, we find that correlations between OND NINO3.4 SSTs and April–May extratropical zonal wind stress are not significant in the TX(WNP) region. It is not clear at this time whether the correlations become insignificant because the signal from the tropics becomes too weak during April–May or whether other sources of variability become too large. The significance of this potential feedback loop is the subject of current research.

Acknowledgments This work was supported in part by a grant from NOAA's Climate Program Office (CLIVAR GC05-170). This study was supported by the Japan Agency for Marine-Earth Science and Technology (JAMSTEC) through its sponsorship of the International Pacific Research Center (IPRC). This is IPRC publication 496 and SOEST publication 7240. We thank two anonymous reviewers and the editor for a careful reading of the manuscript and thoughtful comments.

References

An S-I, Wang B (2000) Interdecadal change of the structure of the ENSO mode and its impact on the ENSO frequency. J Clim 13:2044–2055

Barnett TP, Pierce DP, Latif M, Dommenget D, Saravanan R (1999) Interdecadal interactions between the tropics and midlatitudes in the Pacific. Geophys Res Lett 26:615–618

Behringer DW, Ji M, Leetmaa A (1998) An improved coupled model for ENSO prediction and implications for ocean initialization. Part I: the ocean data assimilation system. Mon Wea Rev 126:1013–1021

Bryan K (1991) Poleward heat transport in the ocean. Tellus 43:104–115

Collins WD, Rasch PJ, Boville BA, Hack JJ, McCaa JR, Williamson DL, Briegleb B, Bitz C, Lin S-J, Zhang M (2005) The formulation and atmospheric simulation of the community atmosphere model: CAM3. J Clim 19:2144–2161

Deser C, Alexander MA, Timlin MS (1996) Upper-ocean thermal variations in the North Pacific during 1970–1991. J Clim 9:1840–1855

Deser C, Phillips AS, Hurrell JW (2004) Pacific interdecadal climate variability: linkages between the tropics and the North Pacific during boreal winter since 1900. J Clim 16:3109–3124

Federov AV, Philander SG (2001) A stability analysis of tropical ocean–atmosphere interactions: bridging measurements and theory of El Nino. J Clim 14:3086–3101

Gu D, Philander SGH (1997) Interdecadal climate fluctuations that depend on exchanges between the tropics and the extratropics. Science 275:805–807

Ji M, Leetmaa A, Kousky VE (1996) Coupled model predictions of ENSO during the 1980s and the 1990s at the National Centers for Environmental Prediction. J Clim 9:3105–3120

Jin F-F (1997) An equatorial ocean recharge paradigm for ENSO. Part I: conceptual model. J Atmos Sci 54:811–829

Johnson GC, McPhaden MJ (1999) Interior pycnocline flow from the subtropical to the equatorial Pacific Ocean. J Phys Oceanogr 29:3073–3089

Joseph R, Nigam S (2005) ENSO evolution and teleconnections in IPCC's twentieth-century climate simulations: realistic representation? J Clim 19:4360–4377

Kleeman R, Power S (1999) Modulation of ENSO variability on decadal and longer timescales. In: Diaz HF, Markgraf V (eds) El Niño and the Southern Oscillation, Multiscale Variability and Its Impacts on Ecosystems and Society. Cambridge University Press, Cambridge, pp 413–442

Kleeman R, McCreary JP, Klinger BA (1999) A mechanism for the decadal variation of ENSO. Geophys Res Lett, 26:743–747

Knutson TR, Manabe S (1998) Model assessment of decadal variability and trends in the tropical Pacific Ocean. J Clim 11:2273–2296

Kraus EB, Turner JS (1967) A one-dimensional model of the seasonal thermocline. II. the general theory and its consequences. Tellus 19:98–106

Latif M, Kleeman R, Eckert C (1997) Greenhouse warming, decadal variability, or El Niño? An attempt to understand the anomalous 1990s. J Clim 10:2221–2239

Liu Z (1999) Planetary wave modes in the thermocline: non-Doppler shift mode, advective mode and Green mode. Quart J Roy Meteor Soc 125:1315–1339

Liu Z, Philander SGH, Pacanowski RC (1994) A GCM study of tropical–subtropical upper-ocean water exchange. J Phys Oceanogr 24:2606–2623

Livezey RE, Chen W (1983) Statistical field significance and its determination by Monte Carlo techniques. Mon Wea Rev 111:46–59

Lu P, McCreary JP (1995) Influence of the ITCZ on the flow of the thermocline water from the subtropical to the equatorial Pacific Ocean. J Phys Oceanogr 25:3076–3088

Lu P, McCreary JP, Klinger BA (1998) Meridional circulation cells and the source waters of the Pacific equatorial undercurrent. J Phys Oceanogr 28:62–84

Lysne J, Chang P, Giese B (1997) Impact of the extratropical Pacific on equatorial variability. Geophys Res Lett 24:2589–2592

McCreary JP, Lu P (1994) Interaction between the subtropical and equatorial ocean circulations: the subtropical cell. J Phys Oceanogr 24:466–497

McPhaden MJ, Zhang D (2002) Slowdown of the meridional overturning circulation in the upper North Pacific. Nature 415:603–608

McPhaden MJ, Zhang D (2004) Pacific Ocean circulation rebounds. Geophys Res Lett 31:L18301. doi:10.1029/2004GL020727

Nitta T, Yamada S (1989) Recent warming of recent sea surface temperature and its relation to northern hemisphere circulation. J Meteor Soc Japan 67:375–382

Nonaka M, Xie S-P (2003) Covariations of sea surface temperature and wind over the Kuroshio and its extension: evidence for ocean-to-atmosphere feedback. J Clim 9:1404–1413

Nonaka M, Xie S-P, McCreary JP (2002) Decadal variations in the subtropical cells and equatorial Pacific SST. Geophys Res Lett 29:1116. doi:10.1029/2001GL013717

Nonaka M, McCreary JP, Xie S-P (2006) Influence of midlatitude winds on the stratification of the equatorial thermocline. J Phys Oceanogr 36:222–237. doi:10.1175/JPO2845.1

Rayner NA, Parker DE, Horton EB, Folland CK, Alexander LV, Rowell DP, Kent EC, Kaplan A (2003) Globel analyses of sea surface temperature, sea ice, and night marine air temperature since the late nineteenth century. J Geophys Res 108(D14):4407. doi:10.1029/2002JD002670

Rothstein LM, Zhang R-H, Busalacchi AJ, Chen D (1998) A numerical simulation of the mean water pathways in the subtropical and tropical Pacific Ocean. J Phys Oceanogr 28:322–344

Schneider NS, Miller AJ (2001) Predicting western North Pacific Ocean climate. J Clim 14:3997–4002

Schneider N, Venzke S, Miller AJ, Pierce DW, Barnett TP, Deser C, Latif M (1999) Pacific thermocline bridge revisited. Geophys Res Lett 26:1329–1332

Shin S, Liu Z (2000) Response of equatorial thermocline to extratropical buoyancy forcing. J Phys Oceanogr 30:2883–2905

Solomon A, McCreary JP, Kleeman R, Klinger BA (2003) Interannual and decadal variability in an intermediate coupled model of the Pacific region. J Clim 16:383–405

Thompson L, Ladd CA (2004) The response of the North Pacific Ocean to Decadal variability in atmospheric forcing: wind versus buoyancy forcing. J Phys Oceanogr 34:1373–1386

Timmermann A, Jin F-F (2002) A nonlinear mechanism for decadal El Niño amplitude changes. Geophys Res Lett 29:1003. doi:10.1029/2001GL013369

Trenberth KE (1990) Recent observed interdecadal climate changes in the northern hemisphere. Bull Am Meteor Soc 71:988–993

Vimont DJ, Battisti DS, Hirst AC (2001) Footprinting: a seasonal connection between the tropics and mid-latitudes. Geophys Res Lett 28:3923–3926

Wang B (1995) Interdecadal changes in El Niño onset in the last four decades. J Clim 8:267–285

Wang D (2003) Entrainment laws and a bulk mixed layer model of rotating convection derived from large-eddy simulations. Geophys Res Lett 30:1929. doi:10.1029/2003GL017869

Wu L, Liu Z, Gallimore R, Jacob R, Lee D, Zhong Y (2003) A coupled model study of Pacific decadal variability: the tropical mode and the north Pacific mode. J Clim 16:1101–1120

Xie S-P, Kunitani T, Kubokawa A, Nonaka M, Hosoda S (2000) Interdecadal thermocline variability in the North Pacific for 1958–1997: a GCM simulation. J Phys Oceanogr 30:2798–2813

Yukimoto S, Endoh M, Kitamura Y, Kitoh A, Motoi T, Noda A (2000) ENSO-like interdecadal variability in the Pacific Ocean as simulated in a coupled general circulation model. J Geophys Res 105:13,945–13,963

Zhang R-H, Rothstein LM, Busalacchi AJ (1998) Origin of upper-ocean warming and El Nino on decadal times scales in the tropical Pacific Ocean. Nature 391:879–883

Zhang D, McPhaden MJ, Johns WE (2003) Observational evidence for flow between the subtropical and tropical Atlantic: the Atlantic subtropical cell. J Phys Oceanogr 33:1783–1797